J Appl Electrochem (2012) 42:699–709
DOI 10.1007/s10800-012-0451-z

ORIGINAL PAPER

Aging of polymer electrolyte membrane fuel cells (PEMFC): general features and investigation of two typical examples

Caroline Bonnet · Ludivine Franck-Lacaze · Bo Tao Huang · Yohann Chatillon · Gérard Valentin · Francois Lapicque

Received: 12 March 2012 / Accepted: 4 July 2012 / Published online: 25 July 2012

Abstract The paper dealing with aging of polymer electrolyte membrane fuel cells is divided in two parts. We present first general comments on the significant issue in an attempt to introduce the topic and to provide basic elements of methodology for investigation: aging mechanisms, reversible or irreversible damage, tests for investigation, and the case of cyclic operations. Then, two examples of cycled operations are presented and discussed for the case of long period cycles—as for day-night applications—operated to single cells. The current density is cycled between two levels in the first example, whereas the second example concerns cycling of relative humidity of inlet air in two fuel cells of different sizes.

Keywords PEMFC · MEA aging · Cyclic operation · Chemical degradation · Electrochemical degradation

1 Introduction

PEM fuel cells are usually considered as reliable tools for energy production for both stationary and mobile application. However, its large-scale industrialization is hindered by two main issues. First, fuel cell cost is often still far too high for possible competition with conventional devices, e.g., internal-combustion engines. DOE target of cost given at \$50/kW in 2010 has been recently announced at \$30/kW by 2015 [1]. The second hindrance is related to durability, i.e., the aptitude to be operated with sufficient efficiency for a long period, and reliability, which can be defined as the capacity of the considered device to be operated without failure. Whereas, the target expressed by DOE in terms of durability is around 40,000 h, the current lifetime of hydrogen fuel cells is estimated at approx. 2,000 h for transport applications, and 10,000 h for stationary power systems [2]. The search for higher durability can be hindered by the search of cheaper and more efficient technologies, involving, for instance, far lower amounts of noble metals or thinner membranes. As a matter of fact, very thin membranes, although exhibiting low electrical resistance, are to suffer more rapidly from chemical or mechanical aging. Likewise, fuel cells provided with electrodes with Pt amounts as low as 10 $\mu g\ cm^{-2}$ can have high performance, but their durability exceed rarely a few hundreds of hours, whereas more robust FC technologies with Nafion 117–type membranes and Pt charges over 1 $g\ cm^{-2}$ have been reported years ago to run for thousands of hours.

In spite of the progresses made during the two last decades, significant R&D investigations have still to be carried out in view to reaching the above cost and durability targets. For this purpose mechanisms of aging processes occurring in fuel cells under nominal operating conditions or under accidental mode have to be better understood. It has been hoped that better knowledge of aging mechanism will lead to more suitable operation of existing fuel cells or FC components, and in a further approach to the design of more efficient FC components or systems. Fuel cell aging has been the topic of various review papers e.g., [3–9] together with other significant papers more focused on membrane degradation, as done for instance by Liu [10] and by Collier et al. [11], or on catalyst aging as described in [12–14]. These great research developments have benefited from the progresses of investigation experimental techniques—chemical analysis, microscopy (SEM, TEM),

C. Bonnet · L. Franck-Lacaze · B. T. Huang · Y. Chatillon · G. Valentin · F. Lapicque (✉)
Reactions and Chemical Engineering Laboratory, CNRS-Université de Lorraine, ENSIC, BP 20451, 54001 Nancy, France
e-mail: francois.lapicque@ensic.inpl-nancy.fr

NMR, Raman or IR spectroscopy, XR diffraction, or XR fluorescence, development of suitable electrochemical techniques e.g., linear or sweep voltammetry, impedance measurements, chronopotentiometry with various current profiles, etc., and by their witty combination for possible evidence of the initiation step in the overall degradation.

The present paper is aimed at presenting in the first part, the elements of the general methodology in fuel cell aging and its investigation. In the second part, two examples of single fuel cell aging are discussed: the first one is a current density cycling and the second one consists in varying the air relative humidity in two different cells. Emphasis is put on the various cross-linked techniques employed for evaluation of the degradation during the long-term runs for the sake of better understanding of the overall degradation.

2 General comments on aging phenomena in fuel cells

Aging phenomena in fuel cell systems can be discussed and evaluated in various manners. The most usual investigation technique consists in examining one cell component concerned by aging, i.e., membrane, catalyst layers, gas diffusion layers or bipolar plates. However, as frequently observed and reported in the relevant literature [3, 5], degradation phenomena seldom occur at one component only, but various parts of the fuel cells can be concerned by aging. For instance, it is known that decomposition of sulfonate-perfluorinated polymers by peroxide-derived radicals is catalyzed by the presence of metal cations even at trace levels. These cations are generated by side dissolution of FC components (Fe and Cu) or by dissolution of Pt clusters upon the action of oxidants such as peroxide radicals (Fig. 1); degradation phenomena of the membrane and Pt catalysts

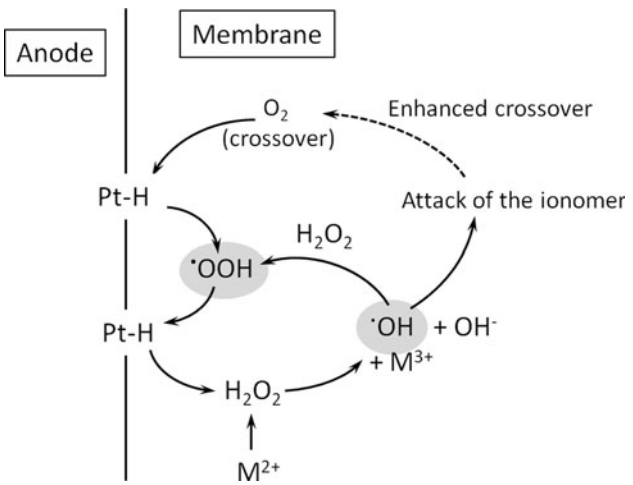

Fig. 1 Formation of active species and radicals for the reduction of crossover oxygen upon catalysis by metal cations (after [3])

then appear as lumped phenomena. Moreover, the presence of oxygen in the anode chamber caused by the gas crossover through the damaged membrane is an additional source of peroxide by reduction with H^+ species. The peroxide formed is known to react with metal cations M^{2+} to generate unstable hydroxide radicals which attack immediately the ionomeric molecule; the enhanced degradation of the membrane results in higher crossover, which accelerates the overall degradation of the membrane electrode assembly (MEA) in a snowball scenario.

Aging phenomena and their investigation can be discussed and classified after various criteria.

2.1 Types of aging

Degradation phenomena of the MEA are often classified into various types, depending on the variable or the properties investigated in the evaluation of the fuel cell or one of its components, as follows:

- Pressure difference between anode and cathode compartments even in the tolerance range given by the supplier is known to favor mechanical degradation. Furthermore, the degradation of the membrane is caused by the finite resistance of the polymer to repeated swelling and shrinking processes occurring under periodic variations of the relative humidity of the feed gases in addition to its progressive thinning. This degradation leads to the formation of cracks, tears, punctures, or pinholes. Moreover, mechanical degradation is also related to the lack of mutual adherence of the various layers—delamination, which hinders the current flow through the cell structure and renders the damaged region little active. Freeze/thaw-cycled operation, for instance, induces both the delamination of the layers and mechanical damage of the polymer bulk.
- Chemical degradation concerns the various components of the cell: decomposition of the polymer, aging of the catalyst through various mechanisms such as Oswald ripening or coalescence of Pt particles, poisoning of the catalyst by gas or liquid contaminants, change in hydrophobicity of the gas diffusion layer (GDL) upon surface oxidation of the carbon-based material, and possible corrosion of bipolar plates. As mentioned above for the case of oxygen crossover, degradation of one cell component can impact on another. The consequences of chemical degradation of the MEA are numerous: reduced conductivity, loss in activity, poorer water management, etc.
- Thermal degradation is caused by excessive temperature and/or insufficient gas humidity; severe dehydration of the polymer results in reduced electrical conductivity and can alter the mechanical properties of the polymeric

foil. Moreover, high gas crossover through the membrane is the cause of local overheating due to catalytic combustion of hydrogen which leads to chemical degradation and amplifies further the significance of the damage.

2.2 Reversibility and significance of the degradation

2.2.1 *Reversibility*

One significant aspect in investigating fuel cell aging is to know whether the observed degradation is reversible or not. Mechanical degradation can be considered as usually irreversible, so can thermal degradation. With concern to chemical degradation, the answer depends on various parameters such as the nature of the degradation agent: oxidative conditions upon presence of oxidants or for too low current density, presence of contaminants, etc. Consider, for instance, the case of contaminants: these species introduced in the fuel cell under operation or produced during its operation can adsorb on the polymeric material or on the metal catalyst. The reversible character of the poisoning depends on the effect of temperature or feeding conditions on the sorption equilibria, i.e., on how easily can the contaminant be released and removed from the ionomer bulk or the catalyst surface. The existence of chemical reactions between the contaminant and the MEA component, e.g., metal sulfide formation in the presence of hydrogen sulfide, is to render the degradation irreversible.

For electrode materials, oxidation of the metal surface, e.g., platinum, can be reversible to some extent, as shown by two examples. First, fuel cell operation at a voltage of 0.8 V or higher results in slow deactivation of the catalyst by oxidation; cyclic operation of the cell at far lower voltage, e.g., 0.5 V, was shown by Uribe and Zawodzinski [15] to regenerate the catalyst. Besides, determination of the active electrochemical area or the fuel crossover by voltammetry in the range 0.05–0.4 V has been reported (see [16] for instance) to regenerate the electrode surface.

2.2.2 *Significance*

The first most basic approach for estimation of the degradation significance consists of comparing the amount of poisoning species to the "substrate" amounts, i.e., the number of ion exchanging or catalytic sites, to be complexed or deactivated, as schematically depicted in Fig. 2. In a more reliable manner, sorption isotherms of the species between the gas or the liquid phase and the membrane or catalyst surface have to be accounted for. For instance, analysis of the work done by Kelly et al. [17] on Nafion membranes contaminated by dilute nickel solutions shows that in all cases, the molar amount of

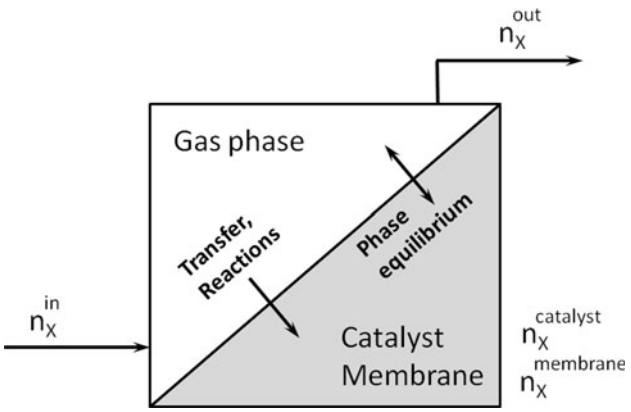

Fig. 2 Contamination of a fuel cell with various amounts η of pollutant (X) at the inlet, the outlet, in the catalyst and, in the membrane structure

Ni^{2+} ions introduced was lower than the membrane capacity. The amounts of cations adsorbed by the membrane varied nearly linearly with the initial concentration in the electrolyte solution being, in addition, close to the initial mass of Ni^{2+} introduced; Ni^{2+} ions thus appear to be preferentially adsorbed on the membrane over H^+ species at all concentration levels, corresponding to a very steep sorption isotherm of the metal cation in the Nafion structure. On the contrary, other contributions have been carried out with large excess of contaminants—often in the fed gases—and analysis of the conclusions reported can indicate on whether the significance of the damage done was limited by the sorption equilibria or be the fact of too short residence times of the gas in the electrode chamber [9]. Finally, as discussed in a former paper for the case of CO-contaminated hydrogen [18], the degradation significance greatly depends on the hydrogen stoichiometry factor. Moreover, the distributions of surface inhibition, overpotential and current density are markedly uneven upon low excess of the reacting gas [18].

2.3 Aging investigation: nominal conditions or use of accelerated tests

For current hydrogen fuel cell technologies, the average decay of the single cell voltage at current densities in the order of 0.5 or 1 A cm^{-2} is in the range 2–10 $\mu V\ h^{-1}$, which corresponds to cell voltage loss from 10 to 50 mV after 5,000 h operation. Operation under less favorable conditions—the presence of contaminants in the gases fed, low current density, inadequate hydration of the cell, etc., is to largely increase the decay rate. Investigation can be conducted until the cell's end of life. However, the so-called end of life does not usually correspond to the utter collapse of the cell, but is defined as the time for which the cell's performance has decreased by 20 %; for galvanostatic runs, this corresponds to 20 % reduction in the cell voltage. In most

cases, the above values show that aging tests under nominal conditions are very long-term experiments.

Because of the long lifetime expectancy of fuel cells, it has appeared necessary to design protocols for accelerated stress tests (AST), which are to indicate the reliability and durability within experiment times far lower than the lifetime under nominal conditions (a time factor from 5 to 20 is often considered). AST may consist of applying potential or humidity cycling, or excessive temperature, in the presence of gas contaminants, or even of ex-situ tests, such as immersion of the cell membrane in Fenton's agent-containing solutions. Accelerated test protocols have to be designed with care so that the conclusions obtained can be transposed to aging under nominal conditions: comparison of the reliability of two cell technologies established from AST experiments have to be representative of that for regular use of the fuel cell. Besides, AST protocols must not induce additional degradation phenomena, which would not be observed in normal operation.

2.4 Aging in cycling operations

Cyclic operations have often been considered to emulate real operations under non-steady state because of the time-depending power demand, or changes in temperature or gas humidification, freeze/thaw operations, etc. In most cases, the variable pulsed in such tests varies between a nominal level and another ("accidental") value for which the cell degradation rate is to be far higher: low or nil current density, zero relative humidity of the inlet gases, transient presence of a contaminant in the fed gases, etc. Besides, repeated cycling from nominal to "accidental" conditions is to induce additional stresses to the various components. For instance, changing the current density level is to change the heat produced by the cell, resulting in changes in local temperature—in spite of the cooling/heating circuit of the fuel cell—and in water management, which is to affect the swelling state of the membrane: in addition to the degradation caused by oxidative conditions, such cycles impact on the membrane's mechanical properties which is also to expand and then to shrink at regular intervals, leading to the formation of cracks or tears and possible local delamination of the electrodes. Therefore, cycling operation affects the cell behavior both by the less favorable conditions in the "accidental" period and by the transient fluctuations of its component properties.

As evidenced by electrochemical impedance spectroscopy (EIS) in fuel cells or any electrochemical process, the various phenomena occurring are of very different characteristic times. Transient charge transport occurs within a few milliseconds or less; charge/discharge of the double layer, in relation to the finite rate of charge transfer at the electrode surface is also fairly rapid, occurs within a fraction of second. In contrast, mass and heat transfer phenomena are far slower: transient of local changes in temperature, concentration, or water content in the membrane has to be observed for periods as long of 1 min or longer. The time lapse of each of the two phases in a test cycle can be compared to the above response time of the various parts of the cells in relation to the physical phenomenon considered.

- Most investigations reported in literature on fuel cells operated under periodic variations of one operating parameter were carried out with fairly short pulsation periods; the time lapse of each phase varied usually from 1 to 20 min. For such pulsations, charge transport and kinetic phenomena are nearly at steady state during the two phases of the cycle, temperature and concentration profiles are in transient regime for a significant fraction of each phase; aging of the fuel cell is due to the less favorable conditions of the "accidental" phase and to the repeated change in physicochemical state of the cell elements concerned by the pulsation.
- On the contrary, for longer periods in each phase of the pulsation—as for instance day-night operation, the transient of all phenomena is of little significance in comparison with the time lapses of each of them: the cell is nearly operated at steady state in each of the two phases, the degradation underwent by the cell being mainly caused by operation during the "accidental" phase of the cycle with little effect of the transient period.

3 Experimental section

3.1 The fuel cells used

The single cell tests were performed with commercial MEAs based on perfluorinated sulfonic acid ionomer reinforced by expanded PTFE being 18-μm thick. For current density tests, the two electrodes were Pt/C with a catalyst loading of 0.4 mg cm^{-2}. For tests with humidity cycles, the anode was Pt/Ru (50:50 at.) at 0.45 mg cm^{-2}, whereas the cathode was the above Pt/C layer. The 310-μm thick gas diffusion layers (SGL 30 BC, UBZM) were dual-layer carbon GDL including a macroporous carbon fiber paper and carbon black microporous layer (MPL). The added hydrophobic PTFE/carbon particles acted as binder. Before cycling operations, each MEA was submitted to maturation at a constant current density and air humidification for 7 days, allowing steady performance to be obtained.

Current density cycling was investigated using 25-cm^2 Electrochem graphite bipolar plates. The pattern of the anode plate was a multiple serpentine one with 0.8 × 0.8 mm linear groove, whereas a column design with squared

$2 \times 2 \times 2$ mm^3 tiles was used as the cathode. Cycling of the relative humidity of the air was investigated with both the above cell and a 100-cm^2 UBZM fuel cell. The bipolar plates of the latter cell were of a carbon-based material with a thinner structure and more water repellent than the above graphite. In addition, the serpentine pattern of the 100-cm^2 anode plate was more sophisticated, whereas the tiles in the cathode plates were 10-mm long and 1.5-mm thick and broad.

3.2 Experimental protocols

The two investigations presented were based on 24-h cycles. Tests with cycled current density were carried out at 65 °C at ambient pressures. In the phases at the nominal current, namely 0.54 A cm^{-2}, air and hydrogen were fed with a stoichiometric factor for the two gases [19]. Air was humidified upstream of the cell at RH = 70 %, whereas dry hydrogen was fed to the anode. The low current density level was fixed at 20 mA cm^{-2} for MEA and 120 mA cm^{-2} for the other. Periods with low current density varied from 2 to 8 h, while periods at 0.54 A cm^{-2} varied from 16 to 22 h. The two MEAs were operated until severe degradation was observed, i.e., for approx. 500 h.

The temperature for tests conducted with air RH pulsation was fixed at 55 °C with a constant current density at 0.3 A cm^{-2} [20, 21]. The stoichiometric factors for hydrogen and air were fixed at 1.5 and 3, respectively. The 24-h cycles consisted of a first 8-h phase with air RH fixed at 62 % and a second 16-h phase with injection of dry air to the cathode. A reference test with constant air humidification was carried out for comparison.

For both type of cycling, electrochemical impedance measurements were carried out at the end of each phase to monitor the state of health of the single cell. Water fractions were collected from the two compartments for chemical analysis by ion chromatography (ICS 300) and estimation of the water transfer coefficient in the cell was done by weighing. Diagnosis of the MEA was achieved at regular intervals by the determination of the hydrogen crossover and the electro active surface area (ESCA) in the cell fed with nitrogen and hydrogen; for fuel crossover, the cell voltage was scanned between 0.05 and 0.6 V at 2 mV/s and the current value at 0.4 V was considered, whereas cyclic voltammetry was carried out in the range 0.05–0.4 V at 50 mV s^{-1} for estimation of the ESCA by integration of the hydrogen desorption peak [22].

4 Current density cycling

Because aging phenomena can be assumed to be of moderate intensity upon operation at 0.54 A cm^{-2}—with a voltage in the order of 0.6 V, the time considered in the whole section was defined as the cumulated time of operation at the low current density level. Run 1, with cycling between 120 and 540 mA cm^{-2} was conducted for 120 h at the low cd, with an overall operation time near 530 h. Run 2, and with cycling between 20 and 540 mA cm^{-2} was conducted for 500 h altogether with 270 h at the lower current density: Run 2 has to be stopped as the cell voltage rapidly decreased toward negative values.

4.1 Cell voltage variation

For the two tests, the voltage recorded at the nominal current density decreased regularly. The rate of voltage decay averaged along the overall run period was estimated at 100 μV h^{-1} for Run 1 and at 180 μV h^{-1} for Run 2. These rates are obviously far larger than the rate indicated by the MEA supplier for operations at regular, continuous operation, in the order of 4 μV h^{-1}. Moreover, for the phases with lower current density level, the cell voltage decreased rapidly depending on the accidental current density (Fig. 3). For current density pulsation between 0.12 and 0.54 A cm^{-2}, the voltage was observed to decay regularly, starting from 0.76 V, with a rate in the order of 100 μV h^{-1}. Upon pulsation at 20 mA cm^{-2}, the cell current decreased from 0.87 V in two phases: (1) for the first 120 h, a steep decay with a rate at 0.7 mV h^{-1} was first observed; (2) then, below 0.77 V, the variation was far slower. Aging phenomenon then appears to be greatly dependent on the cell voltage—with smaller influence from the current density—and with sort of transition near 0.77 V for the cell technology employed here.

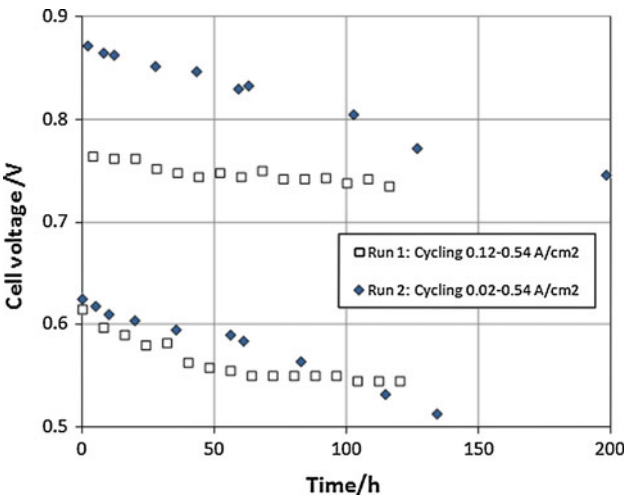

Fig. 3 Time variation of the cell voltage for the tests with pulsed current density from 0.54 to 0.12 A cm^{-2} (Run 1) and from 0.54 to 0.02 A cm^{-2} (Run 2)

4.2 Chemical degradation of the membrane

The degradation of the catalyst is not described here. More emphasis is put on the membrane degradation.

From the water fractions collected, ICP-MS measurements could not yield the concentrations of platinum species in the liquid fractions since the signal observed was only in the order of the detection threshold, at 0.01 mg L^{-1}. On the contrary, the presence of sulfate and fluoride ions was detected in all fractions, indicating the degradation of the ionomer [23–26]; whereas the presence of sulfate results from the cleavage of ion-exchanging side chain of the polymer, fluoride can be formed by both cleavage of the side chain and unzipping of the polymer backbone via weak-end groups [26]. On the basis of the Nafion formula usually considered in literature [27], each side chain contains ten atoms of F and one sulfonate group, whereas the monomer backbone contains 29.24 F atoms, regardless of the above side chain.

Although higher concentrations of the two ions were usually found in the anode side, for the sake of simplicity here, average concentrations in the cell were calculated taking into account the flow rates of water collected from the anode and cathode compartments.

4.2.1 Loss in sulfur

For the two runs, the sulfate concentration was in the order of 0.3 mg L^{-1}, for which the signal-over-noise ratio was not always large than 10; the uncertainty in sulfate determination was therefore estimated at 25 % [19]. Nevertheless, the time profiles presented in Fig. 4 show that the rate of side-chain cleavage remained nearly constant during the long-term cycling runs, regardless of the current density; for the two MEAs tested, the loss in sulfonate group was in the order of 10 % within the approx. 500 h of the runs, corresponding to a rate of side-chain cleavage of 0.02 % h^{-1}. Reference tests conducted at 540 mA cm^{-2} revealed negligible amounts of sulfate, i.e., in the order of the signal-to-ratio threshold, corresponding to sulfonate losses below 0.004 % h^{-1}. Cycling current density was then shown to induce appreciable side-chain cleavage; the process once initiated does not seem to stop in periods when the current density returns to its normal level.

4.2.2 Loss in fluorine and attempts of interpretation

Contrary to what was observed for sulfate, the profiles of fluoride concentration varied greatly with time with a strong influence of the current density, as explained below. The first three cycles in Run 1 with low fluorine concentrations induced the membrane degradation to be started. Then, until cycle 8, the concentration was in the range 1–2 mg L^{-1} in both cycle phases (Fig. 5a), corresponding to around 10^{-4} mol L^{-1} fluoride ions, whereas the sulfate concentration was near 3–4 10^{-6} mol L^{-1}. In this part of Run 1, the F/S atom ratio was in the range 25–40, indicating that the polymer degradation is the fact due to both unzipping of the chain backbone and cleavage of the side chain. After cycle 8, [F^-] remained constant regardless of the current density level at around 0.5 mg L^{-1}, i.e., 2.6 10^{-5} mol L^{-1}, corresponding to F/S ratios near 10 or below: in the last part of Run 1, cleavage of the side chain seems to be the predominant reaction in the degradation. The change in reaction mechanism along the run might be attributed to the different reactivity of the monomers—which seems unlikely considering the regular structure of the backbone—or to the lower cell voltage and cathode potentials in the final part of the run than in the first cycles.

The striking difference exhibited by Run 2 is that the fluoride concentration was ruled by the current density levels (Fig. 5b); [F^-] values in the liquid fractions recovered at 20 mA cm^{-2} were 3–5 times larger than the concentration in the liquid collected in the preceding phase at nominal current density. Besides, the membrane chemical degradation proceeds in three steps as follows. The induction period for the three first cycles was followed by a phase of intense degradation with fluoride concentration over 15 mg L^{-1} at 20 mA cm^{-2}; during the two last cycles before the MEA collapse, F^- concentration was at more reasonable levels (Fig. 5b), even in the (accidental) low current density periods. The latter reduction in chemical degradation rate is

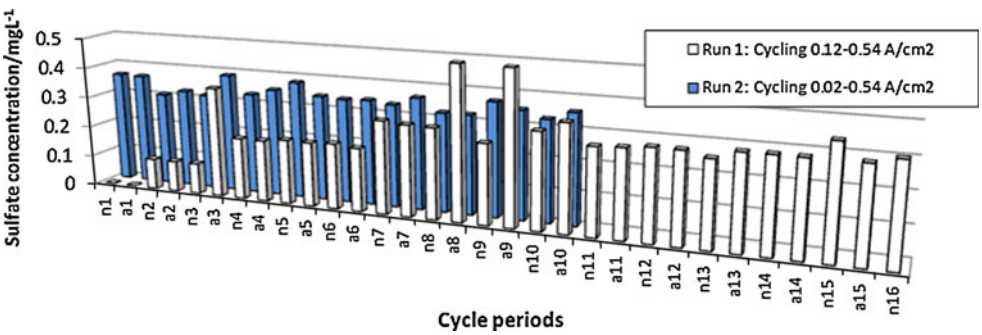

Fig. 4 Concentration of sulfate ions in the collected water fractions resulting from sulfonate loss from the membrane structure during the tests with pulsed current density from 0.54 to 0.12 A cm^{-2} (Run 1) and from 0.54 to 0.02 A cm^{-2} (Run 2). Nominal conditions are referred by "n," whereas "a" is for accidental conditions

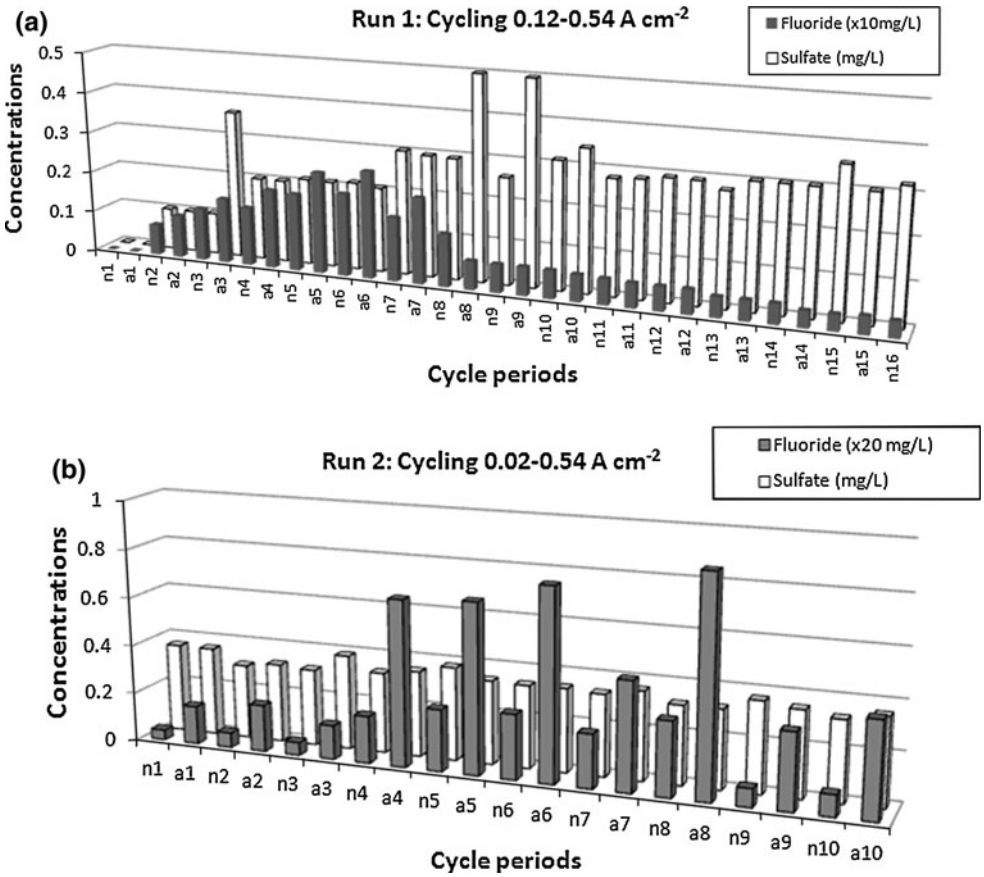

Fig. 5 Concentration of fluoride ions in the collected water fractions collected resulting from fluorine loss from the membrane structure during the tests with pulsed current density from 0.54 to 0.12 A cm^{-2} (**a**) and from 0.54 to 0.02 A cm^{-2} (**b**). Nominal conditions are referred by "n," whereas "a" is for accidental conditions

probably linked to the lower cell voltage (Fig. 4) corresponding to less aggressive conditions during the last part of the run, as mentioned above. The F/S ratio was in all periods of the run far larger than 10. Although side chain cleavage likely occurs, unzipping of the ionomer backbone represents a significant degradation reaction, in particular, in periods at 20 mA cm^{-2} for which the F/S ratio could largely exceed 100. The loss in fluorine species from the membrane was estimated to 11.9 % in Run 2 far larger than that for Run 1 (3 %).

5 Relative humidity cycling

As explained in Sect. 3, tests have been carried out with two single cells, the area of which was 25 and 100-cm^2, respectively, although with the same MEA and GDL. For the smaller cell, the run had to be stopped after 27 cycles (approx. 600 h) because of sudden cell failure; the larger cell could be operated for a longer period and was stopped after 1,150 h.

5.1 Cell voltage

For the two cells, higher voltages were obtained in the periods with humidified air (RH = 62 %). Nevertheless, the voltage profiles recorded along the run differed significantly from one cell to the other (Fig. 6). The voltage at nominal conditions varied regularly along time with average decay rate of 33 μV h^{-1} for the smaller cell and 60 μV h^{-1} for the larger cell. The main difference between the two variations concerns operation with dry air injection. For the smaller cell, this potential variation exhibited three periods: for the first ten cycles, the voltage at RH = 0 % was fairly constant although 90 mV below its level upon air humidification;

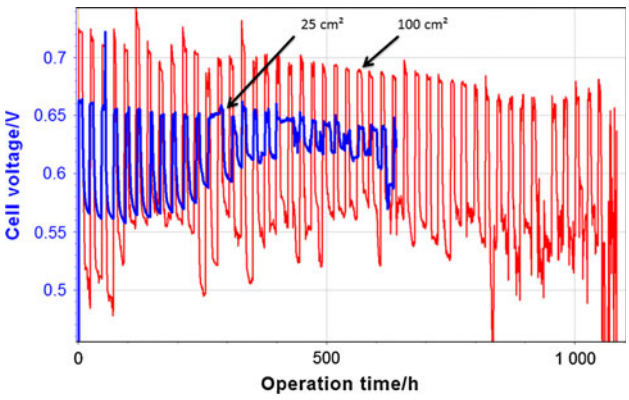

Fig. 6 Time variation of the cell voltage for the tests with pulsed relative humidity in fed air (0–62 %) in the 25 and 100 cm^2 PEM cells

then, the voltage at RH = 0 % increased regularly so that the amplitude of the pulsed variation decreased to 40 mV (Fig. 6). After cycle 18, the voltage difference remained constant until a significant voltage decay in the last cycles before the MEA collapse. For the larger cell, the amplitude of the voltage variations was in the range of 120–200 mV along the run. Moreover, high fluctuations of the cell voltage in the dry periods were observed for the last cycles of the run (Fig. 6); this fluctuation could be attributed to non-satisfactory water management.

5.2 Fuel crossover

Figure 7 shows the very different variations of the fuel crossover—expressed as a current density of hydrogen oxidation—of the two cells. For the smaller one, the crossover increases nearly exponentially along the run, as indicated by the semi-log plot, attaining 95 mA cm^{-2} for the last cycle. This value corresponds approximately to one-third of the current density and the excess of hydrogen, which is likely the cause of the cell starvation during the following cycle. For the 100-cm^2 cell, RH cycling has a less significant effect on the fuel crossover, which slightly increased from 1.8 mA cm^{-2} only after cycle 31 (approx. 750 h) to attain <4 mA cm^{-2} at the end of life of the MEA (Fig. 7).

5.3 Water management and ohmic resistance

Water management in the cell can be characterized by the water amount in the outlet gases in comparison with the humidification conditions. This water amount was estimated by cooling the gas in a heat exchanger and weighing the fractions recovered. It was expressed by factor W which is defined as the amount of water collected to the amount contained in the same flow rate of gas saturated with water at the cell temperature; liquid water is present in the cell for W larger than unity. Variations of factor W are shown in Fig. 8; the two cells exhibit different

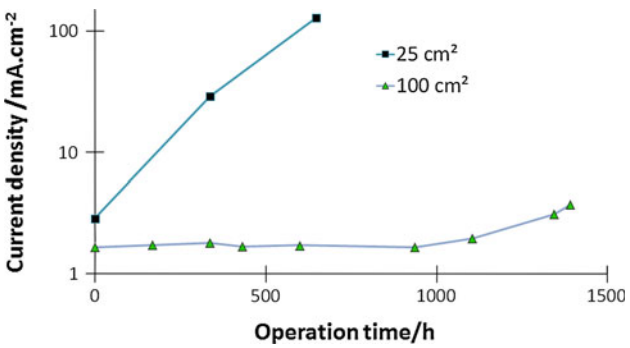

Fig. 7 Fuel crossover for the tests with pulsed relative humidity in fed air (0–62 %) in the 25 and 100 cm^2 PEM cells

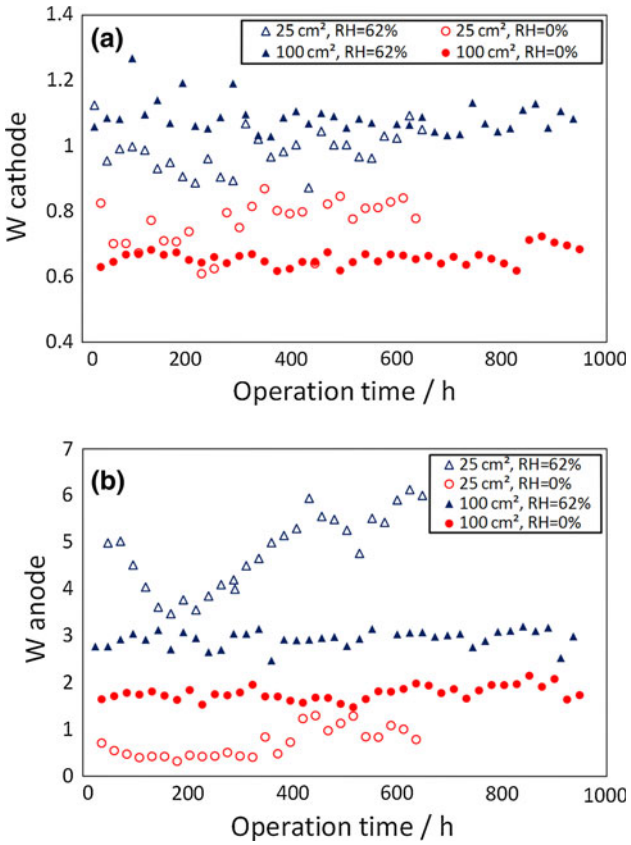

Fig. 8 Amount of water at the outlet of the cell normalized by the water amount corresponding to saturation conditions for the tests with pulsed relative humidity in fed air (0–62 %) in the 25 and 100 cm^2 PEM cells. **a** Cathode side, **b** anode side

behaviors as explained below. As expected, coefficient W is larger in the periods with humidified air than upon dry air feeding. At the cathode outlet, W exceeds unity in the larger cell, being 1.09 within 5 %, whereas no—or very little—liquid water is formed in the cathode compartment of the smaller cell since W is near 1 within 8 % (Fig. 8a). With respect to the anode side, the moderate excess of hydrogen renders the flow rate of the outlet gas far lower than that of the inlet gas, which results in high values of coefficient W. As shown in Fig. 8b, the outlet of the 25-cm^2 anode compartment is liquid water free for the 25-cm^2 cell during the dry air injection periods (W = 0.72 within 44 %), whereas liquid water is formed in the anode chamber of the larger cell in both periods of the cycle—although in different proportions. By a compensation effect, the outlet gas of the 25-cm^2 anode has a larger liquid amount than that issued from the larger anode.

Water management was also studied in terms of water transport coefficient α, which is defined for the present case of dry hydrogen fed to the anode, as the ratio of the water amount recovered from the anode side over the quantity of water produced in the cell. The variation of the coefficient

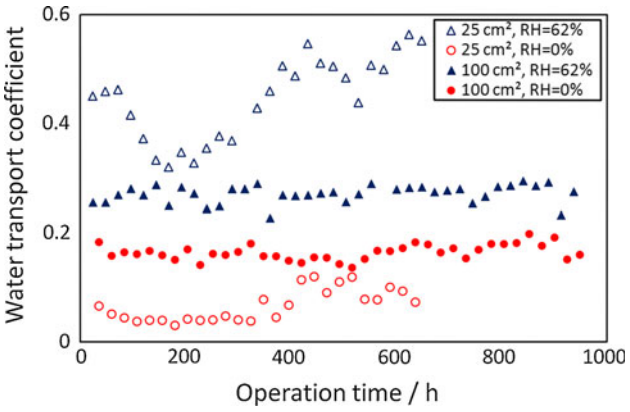

Fig. 9 Water transport coefficient to the anode side for the tests with pulsed relative humidity in fed air (0–62 %) in the 25 and 100-cm^2 cells

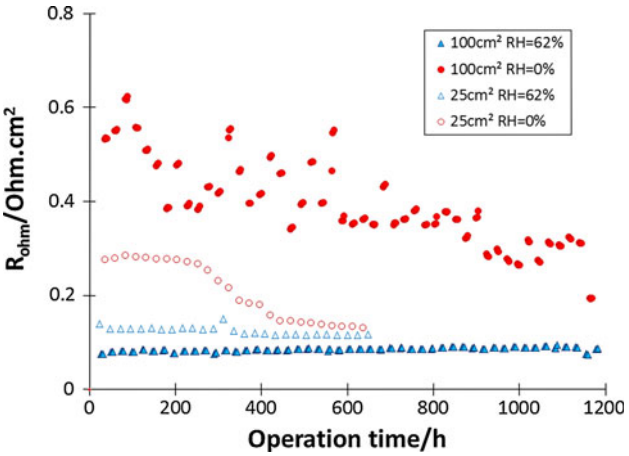

Fig. 10 Ohmic resistance of the 25- and 100-cm^2 cells for the tests with pulsed relative humidity in fed air (0–62 %)

is given in Fig. 9. In consistence with the data of Fig. 8a, the smaller cell exhibits sharper differences in α coefficient between dry and humidified periods with average values at 0.07 and 0.42 for RH = 0 and 62 %, respectively. For this cell, α tends to increase after cycle 10 (240 h), which could be linked to the increased gas permeation modifying water management in the cell; for the last cycles, the high "porosity" of the membrane is the source of higher water transport from the cathode to the anode in a large part of the cell. On the contrary, in the 100-cm^2 cell, the water transport coefficient remains constant—in accordance with the little significant convection between the two compartments—and at more comparable values (0.15 and 0.27 for RH = 0 and 62 %, respectively).

For the two cells operated with nominal air humidification, the ohmic resistance of the two cells varied quite little along the aging runs (Fig. 10). Examination of Figs. 8a and 10 shows that the ohmic resistance (in Ohm cm^2) is as much larger as the hydration coefficient W at the cathode is low: this can partly explain why the smaller cell exhibits a higher resistance than the larger one for RH = 62 %. During the periods with the injection of dry air, the cell resistance is noticeably higher, expected. For RH = 0 %, the ohmic resistance exhibited by the two cells decreases with the same rate, near 6.5 m Ohm cm^2 per cycle, although its corresponding initial values are very different. The electrical behavior of the cells operated with dry air tends to become closer to that observed with RH = 62 %, in particular for the 25-cm^2 cell, for which the resistance difference between dry and humid periods is only at 10 % at the end of the run (Fig. 10).

5.4 Electrochemical characterization

Direct comparison of the electrochemical surface area (ECSA) of the two MEAs could not be achieved directly because of their different initial value although from the same supplier. Only the cathode side was investigated here. ECSA of the 25-cm^2 cathode was found at 274-cm^2 Pt cm^{-2}, whereas the area of the larger cathode was near 252-cm^2 Pt cm^{-2}. As shown in Fig. 11, the two surface areas regularly decreased along the run. For the smaller cell, the standardized ECSA decreased with a fairly constant rate of 1 % per cycle (per day) until the MEA collapsed. The surface area in the larger cell varied somewhat differently, exhibiting a higher rate until cycle 18 at 1.8 % per day, then a smaller rate near 0.4 % per day until the end of the run.

The charge transfer resistance of the two cell cathodes, R_{ct}, was largely affected by the air humidification: lower resistances were found with RH = 62 % (Fig. 12). As reported in [28, 29], high hydration condition results in higher conductivity of the thin ionomeric layer, allowing easier transfer of protons to Pt clusters for oxygen reduction, resulting in overall improved reaction rates. For nominal humidification (RH = 62 %), the two cells exhibited similar charge transfer resistance. In the period of dry air injection, the charge transfer resistance was observed to decrease regularly for the first 20 cycles in both cells, in spite of strong

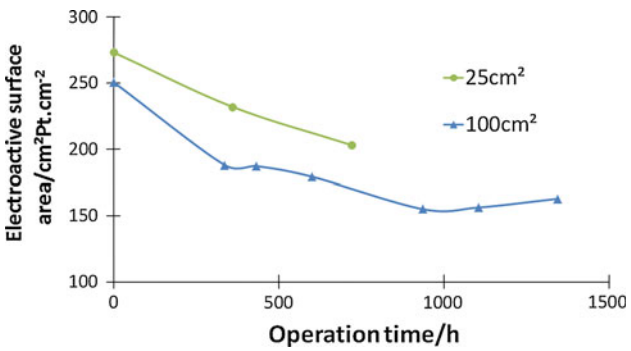

Fig. 11 Electrochemical surface area (ESCA) of the cathode of the 25- and 100-cm^2 cells for the tests with pulsed relative humidity in fed air (0–62 %)

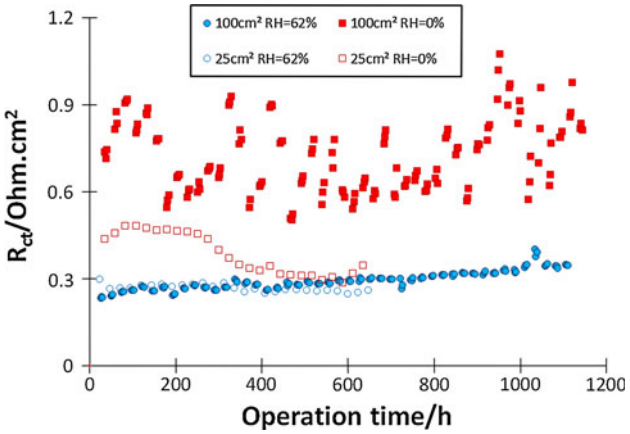

Fig. 12 Charge transfer resistance of the cathode in the 25- and 100-cm^2 cells for the tests with pulsed relative humidity in fed air (0–62 %)

data scattering for the larger cell; this noticeable trend is also linked to the improvement of humidification of the cathode discussed in Sect. 5.3. As for the ohmic resistance, and because of the most significant fuel crossover during the last cycles, the electrochemical behavior of the 25-cm^2 cell was little modified by the change in RH. In contrast, the charge transfer resistance of the larger cell for RH = 0 % was found to increase linearly, in particular, from cycle 30 (720 h); in spite of the slightly improved hydration of the large cathode, the significant reduction in ECSA (Fig. 11) is to result in an overall reduction in the rate of oxygen reduction, expressed by higher charge transfer resistances.

The above difference in behavior of the two cells was also observed by comparison of the diffusion resistance at the cathode, R_{diff}, with far higher values obtained for the larger cell in both phases of the RH cycle (Fig. 13). In periods with RH = 62 %, the value of the humidity factor W is in the order of unity, corresponding to nil or little significant amount of liquid water; mass transfer

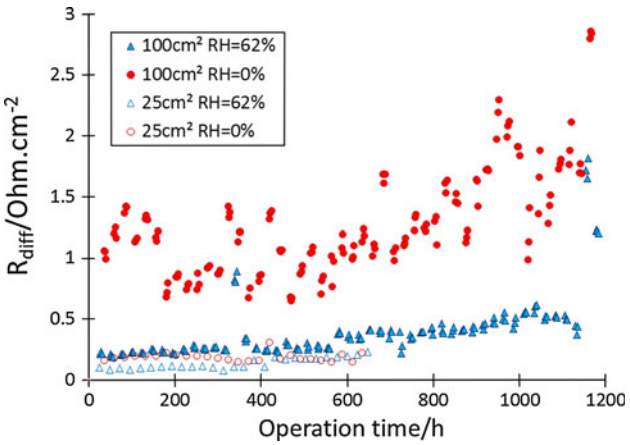

Fig. 13 Diffusion resistance of the cathode in the 25- and 100-cm^2 cells for the tests with pulsed relative humidity in fed air (0–62 %)

phenomena are not hindered in these periods in comparison to what occurs during the dry periods. Surprisingly, very high values of this resistance have been observed under dry air injection into the larger cathode, in particular, at the end of the run (Fig. 13).

5.5 Discussion

The diverging behavior exhibited by the two cells mounted with the same GDL and MEA is not directly related to a scale effect. The observed phenomenon is probably linked to difference in water management in the cell. First, the poorer hydrophobicity of the 25-cm^2 bipolar plates renders less efficient removal of liquid water from the fuel cell structure and maintains sufficient hydration in the MEA. Besides, the different dimensions of the tiles in the column-patterned anodes can also contribute to the observed divergence. In the smaller cell, the large periodic change in water transport coefficient and coefficient W at the anode by RH cycling are to induce very significant shrinking and swelling phenomena of the membrane; the most severe mechanical stress generated results in greatly increased crossover and modified water management in the cell. On the contrary, both flow patterns and material of the bipolar plates in the 100-cm^2 cell are more favorable to water removal from the cell. Further investigations consisting in measurements of the contact angle of the various plates [30]—before and after the run—together with computational fluid dynamics of the two phase flows would be required for thorough understanding of the overall aging phenomena.

6 Conclusion

Aging phenomena have to be considered as a whole in fuel cell investigations, either under operation or in postmortem analysis. Description of the various aging phenomena can be afforded by extensive, combined use of various experimental techniques together with elements of chemical engineering. The two examples of 24 h-cycling experiments presented here illustrates different aging phenomena, which are often linked to each other only. For the case of repeated high cathode potentials, in addition to oxidation of the catalyst and the surface properties of both GDL and bipolar plates—with reduced hydrophobicity—the polymer was shown to suffer from various degradation mechanisms depending on the cathode potential level. Moreover, repeated injection of dry air to the cathode changes dramatically the water management, affects the mechanical properties of the membrane, and reduces the electrochemical active area of the catalyst. However, for the two cells investigated, with different areas, designs, and materials of the bipolar plates,

very different behavior along RH cycling has been observed, probably due to the very different hydrophobicity and water management in the cells.

Acknowledgments The investigations have been partly funded by the French Research National Agency (ANR) within the DamaS project (ANR JCJC). Several facilities used in the investigations have been subsidized by the *Contrat de Projet Etat-Région Lorraine "Piles à Combustible. Interface pour le transport terrestre."*

References

1. Wang Y, Chen KS, Mishler J, Cho SC, Cordobes Adroher X (2011) Appl Energy 88:981
2. Payne T (2009) Fuel cells durability and performance. The Knowledge Press Inc, US Brookline
3. Borup R, Meyers J, Pivovar B, Kim YS, Muikundan R, Garland N, Myers D, Wilson M, Garzon F, Wood D, Zelenay P, More K, Stroh K, Zawodzinski T, Boncella J, McGrath JE, Inaba M, Miyatake K, Hori M, Ota K, Ogumi Z, Miyata S, Nishikata A, Siroma Z, Uchimoto Y, Yasuda K, Kimijima K, Iwashita N (2007) Chem Rev 107:3904
4. Schmittinger W, Vahidi A (2008) J Power Sources 180:1
5. Zhang S, Yuan XZ, Wang HJ, Merida W, Zhu H, Shen J, Wu SH, Zhang JJ (2009) Int J Hydrogen Energy 34:388
6. de Bruijn FA, Dam VAT, Janssen GJM (2008) Fuel Cells 08(1):3
7. Wang Y, Chen KS, Mischler J, Cho SC, Cordobes Adroher X (2011) Appl Energy 88:981
8. Yu Y, Li H, Wang H, Yuan X-Z, Wang G, Pan M (2012) J. Power Sources 205:10
9. Lapicque F, Bonnet C, Huang BT, Chatillon Y (2012) "Analysis and evaluation of aging phenomena in PEMFCs" Chapter 5 in « Fuel cell engineering: model-based approaches for analysis, control and optimization. In: Sundmacher K (ed) Advances in chemical engineering series. Elsevier, Amsterdam
10. Liu W, Ruth K, Rusch G, Mater JN (2001) Electrochem Syst 4:227
11. Collier A, Wang HJ, Yuan XZ, Zhang JJ, Wilkinson DP (2006) Int J Hydrogen Energy 31:1838
12. Ferreira PJ, Ia O'GJ, Shao-Horn Y, Morgan D, Makharia R, Kocha S, Gasteiger HA (2005) J Electrochem Soc 152:A2256
13. Guilminot E, Corcella A, Charlot F, Maillard F, Chatenet M (2007) J Electrochem Soc 154:B96
14. Wu JF, Yuan XZ, Martin JJ, Wang H, Zhang J, Shen J et al (2008) J Power Sources 184:104
15. Uribe FA, Zawodzinski TA (2002) Electrochem Acta 47:3799
16. Cleghorn SJC, Mayfield DK, Moore DA, Moore JC, Rusch G, Sherman TW, Sisofo NT, Beuscher U (2006) J Power Sources 158:446
17. Kelly MJ, Fafilek G, Besenhard JO, Kronberger H, Nauer GE (2005) J Power Sources 145:249
18. Bonnet C, Franck-Lacaze L, Ronasi S, Besse S, Lapicque F (2010) Chem Eng Sci 65:3050
19. Franck-Lacaze L, Bonnet C, Choi E, Moss J, Pontvianne S, Poirot H, Datta R, Lapicque Int F (2010) J Hydrogen Energy 35:10472
20. Huang BT, Chatillon Y, Bonnet C, Lapicque F, Leclerc S, Hinaje M, Raël S (2012) Fuel Cells 12(3):335
21. Huang BT, Chatillon Y, Bonnet C, Lapicque F, Leclerc S, Hinaje M, Raël S (2012) Fuel Cells 12(3):347
22. Pozio A, De Franceco M, Cemmi A, Cardellini F, Giorgi L (2002) J Power Sources 105:13
23. Chung CG, Kim L, Sung YW, Lee J, Chung JS (2009) Int J Hydrogen Energy 34:8974
24. Ohma A, Yamamoto S, Shinohara K (2008) J Power Sources 182:39
25. Wang F, Tang HL, Pan M, Li DX (2008) Int J Hydrogen Energy 33:2283
26. Xie T, Hayden CA (2007) Polymer 48:5497
27. Shah AA, Ralph TR, Walsh FC (2009) J Electrochem Soc 156:B465
28. Zhang JL, Tang YH, Song CJ, Xia ZT, Li H, Wang HJ, Zhang JJ (2008) Electrochim Acta 53:5315
29. Kim HT, Song KY, Reshetenko TV, Han SI, Kim TY, Cho SY, Min MK, Chai GS, Shin SC (2009) J Power Sources 193:515
30. Cho EA, Jeon U-S, Hong S-A, Oh I-H, Kang S-G (2005) J Power Sources 142:177